12th International Symposium on Turbulence and Shear Flow Phenomena (TSFP12)
Osaka, Japan (Online), July 19-22, 2022

INHOMOGENEOUS TURBULENCE SCALINGS IN A FREE SHEAR FLOW

F. Alves Portela
Laboratoire de Mécanique des Fluides de Lille
Univ. Lille, CNRS, ONERA, Arts et Métiers ParisTech, Centrale Lille
Kampé de Feriet, 59000 Lille, France
felipe.alvesportela@univ-lille.fr

J. C. Vassilicos
Laboratoire de Mécanique des Fluides de Lille
Univ. Lille, CNRS, ONERA, Arts et Métiers ParisTech, Centrale Lille
Kampé de Feriet, 59000 Lille, France
john-christos.vassilicos@centralelille.fr

ABSTRACT

We explore the dependence of the normalised turbulence dissipation rate C_ε on the local Taylor length-based Reynolds number Re_λ and its relation to two-point statistics, using DNS data of planar wakes generated by pairs of square prisms. Power laws relating C_ε and Re_λ are found across the whole breadth of the wake as well as in the direction of the mean flow. A recent theory of inhomogeneous turbulence is confronted to this dataset. In the case where the two square prisms are not too close to each other, the theory provides satisfactory collapse of the second order structure functions even where the turbulence is highly inhomogeneous. Our results suggest that the theory could benefit from explicitly incorporating mean flow inhomogeneity in order to broaden its applicability, since we find the largest Reynolds numbers precisely where the mean flow is most inhomogeneous.

INTRODUCTION

In free shear flows such as turbulent wakes, intense turbulence is produced by immersing solid bodies in an otherwise undisturbed flow. The resulting flows are often populated by coherent structures which interact with the turbulence in a non-trivial manner, introducing long range correlations, both in space and time. The turbulent cascade that ensues is fundamentally different from the classical homogeneous, isotropic and statistically stationary cascade (Thiesset & Danaila, 2020).

There is, however, some common ground between these two classes of turbulence: most notably, the infamous $-5/3$ spectral power law of the velocity spectrum which has been reported in a plethora of flows where the turbulence is demonstrably non-conforming with the assumptions involved in the classical theory of Kolmogorov (Kraichnan, 1974; Alves Portela *et al.*, 2017).

Such departure from a classical cascade is encapsulated in the dependence of the normalised dissipation $C_\varepsilon = \varepsilon \mathscr{U}^3/\mathscr{L}$ on global and local Reynolds numbers

$$C_\varepsilon \propto \left(\frac{\sqrt{Re_\infty}}{Re_\lambda}\right)^p, \tag{1}$$

which reflects the non-equilibrium between inertial range energy exchanges and the turbulence dissipation rate.

The non-equilibrium relation given by eq. (1) has been reported in a broad variety of flows (see Vassilicos, 2015; Ortiz-Tarin *et al.*, 2021, and references therein) by probing the concurrent evolution of C_ε and Re_λ (the local Taylor length-based Reynolds number) in the direction of the mean flow or in time. Recently, however, Chen *et al.* (2021) reported $C_\varepsilon \propto Re_\lambda^{-1.5}$ by measuring those two quantities along the breadth of planar wakes generated by pairs of square prisms. In a follow-up work, Chen & Vassilicos (2022) presented a theory of inhomogeneous turbulence which retrieves the $2/3$ scaling of the second order structure function by taking into account the spatial inhomogeneity of C_ε and Re_λ:

$$\delta u^2 = k\left(\frac{r}{\mathscr{L}}\right)^{2/3} f\left(\frac{r}{\ell_i}\right). \tag{2}$$

This scaling is different from the Kolmogorov scaling $(\varepsilon r)^{2/3} f(r/\eta)$ because ε does not scale as $k^{3/2}/\mathscr{L}$. The authors also argue that eq. (2) could hold both for the stream-wise and cross-stream velocity components, respectively u_1 and u_2, which they confirm with their experiments, so long as mean flow inhomogeneity is not significant.

The theory of Chen & Vassilicos (2022) makes use of a generalised scale-by-scale energy budget which distinguishes between exchanges in physical (X) and scale space (r)

$$\underbrace{\langle\sigma u_i\rangle\frac{\partial\langle(\delta u_1)^2\rangle}{\partial X_i}}_{\mathscr{A}_u} + \underbrace{\frac{\partial\langle\delta u_i(\delta u_1)^2\rangle}{\partial r_i}}_{\Pi_u} = \underbrace{-\frac{\partial\langle\sigma u_i'(\delta u_1)^2\rangle}{\partial X_i}}_{\mathscr{T}_u} + \underbrace{+2\langle\delta u_1\frac{\partial\delta p}{\partial X_1}\rangle}_{\mathscr{T}_{p,u}} + \underbrace{\nu\frac{1}{2}\left(\frac{\partial}{\partial X_i^2}+\frac{\partial}{\partial r_i^2}\right)\langle(\delta u_1)^2\rangle}_{\mathscr{D}_u} - \sigma\varepsilon_1, \tag{3}$$

where the σ and δ symbols denote the two-point half-sum and half-difference, respectively, and $u_i = \langle u_i\rangle + u_i'$. Inner and

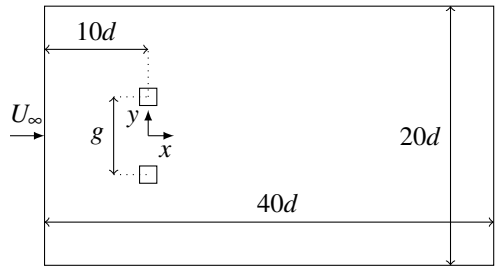

Figure 1: Problem dimensions in terms of the squares size d.

outer length scales ℓ_i and $\mathscr{L}$) are then introduced to establish inner and outer balances from eq. (3). By introducing some assumptions on the structure of these balances and requiring dissipation to scale both in terms of inner and outer quantities (all of which effectively replace Kolmogorov's similarity hypotheses) one can then obtain eq. (2).

In the present contribution, DNS of planar wakes generated by pairs of square prisms at $Re_\infty = 5000$, for two different spacings between the prisms, were carried out. This database allows us to see some of the boundaries of applicability of the theory introduced in Chen & Vassilicos (2022) by accessing information not available to Chen *et al.* (2021) such as the full velocity gradient tensor and the out-of-plane velocity component. This allows us to go beyond the experiments by directly computing all the terms involved in eq. (3).

NUMERICAL SETUP

The incompressible Navier-Stokes equations are solved using Incompact3d, an open-source solver developed by Bartholomew *et al.* (2020). The spatial discretisation uses 6th order compact differences whereas the time integration is carried out with a 3rd order Adams-Bashfort scheme. Stability of the numerical solution is ensured by selectively introducing numerical dissipation as described in Lamballais *et al.* (2011). The no-slip condition is enforced through the immersed boundary method as in Gautier *et al.* (2014).

The set-up used in this work is similar to that of Zhou *et al.* (2019) with a geometry as illustrated in fig. 1. Uniform velocity U_∞ is imposed at the inlet whereas the outlet is treated with a convective boundary condition (using the maximum velocity normal to the outlet for the convective velocity). Periodicity is enforced at the cross-flow boundaries which are $20d$ apart. The span-wise direction is πd wide and is also treated as periodic. The global Reynolds number is $Re_\infty = U_\infty d/\nu = 5000$, where ν is the kinematic viscosity. The gap ratios g/d simulated are 1.25 and 2.4.

For both gap ratios considered, the above configuration led to a resolution varying between 2η and 6η, typically of $\mathscr{O}(3\eta)$, with η being the Kolmogorov length scale. The shedding frequency, taken as that where the power spectral density of u_2' (fluctuating velocity in the y direction) is maximal, for the $g/d = 1.25$ and $g/d = 2.4$ were found to be $0.08U_\infty/d$ and $0.16U_\infty/d$, respectively, leading to a sampling time of *ca.* 180 and 420 shedding cycles, respectively.

RESULTS

The Normalised Turbulent Dissipation

We start by investigating how the normalised turbulence dissipation rate

$$C_\varepsilon = \varepsilon \frac{\mathscr{U}^3}{\mathscr{L}} \tag{4}$$

depends on the local Reynolds number

$$Re_\lambda = \frac{\mathscr{U}\lambda}{\nu} \tag{5}$$

with the Taylor micro-scale defined as $\lambda = \sqrt{15\frac{\nu}{\varepsilon}\frac{\mathscr{U}^2}{3}}$.

The choice of velocity and length scales for eqs. (4) and (5) follows that of Chen *et al.* (2021). Namely, the velocity scale $\mathscr{U}$ is taken as $\langle\sqrt{u_i'u_i'}\rangle$ whereas the length scale $\mathscr{L}$ is obtained by integrating the stream-wise autocorrelation function of u_2' up to its first zero crossing.

In Chen *et al.* (2021), the turbulence dissipation, which is involved in eq. (4) directly and in eq. (5) through λ, was computed using the assumption of small-scale axisymmetry (see George & Hussein, 1991). Our DNS suggests (not shown here for brevity) that this assumption yields very good estimates of ε, perhaps even slightly better than small-scale isotropy (for the $g/d = 2.4$ case in particular) which also yields good dissipation estimates. We also found that computing $\mathscr{L}$ from the stream-wise autocorrelation function of u_3 does not alter any of our conclusions.

We find that both C_ε and Re_λ vary significantly along x and y, for both gap ratios considered here. As seen in fig. 2, the stream-wise evolution of C_ε and Re_λ is drastically different between configurations: while Re_λ increases with x for $g/d = 1.25$ it decreases for $g/d = 2.4$, conversely C_ε decreases with x for $g/d = 1.25$ and increases for $g/d = 2.4$. Looking at the product $C_\varepsilon Re_\lambda$ along x (fig. 3) reveals that the nonequilibrium scaling $C_\varepsilon \propto Re_\lambda^{-1}$ holds only for $g/d = 2.4$ as for $g/d = 1.25$ C_ε decreases faster with x than the increase in Re_λ.

The y extent in Chen & Vassilicos (2022) where C_ε and Re_λ were measured was restricted to $|y| < 0.5d$. Here we examine these two quantities throughout the whole breadth of the wake. Specifically, at a given x location, we consider all y locations where the mean enstrophy is larger than $1/4$ the maximum mean enstrophy at that x location, as illustrated in fig. 4.

In fig. 5 we plot C_ε versus Re_λ within the whole wake for $x > 10d$; it can be clearly seen that these two quantities are related through power laws of the type $C_\varepsilon \propto Re_\lambda^{-p}$. For $g/d = 1.25$ we find $p \approx 1.3$ from $x = 10d$ onwards, whereas in the $g/d = 2.4$ configuration p gradually increases from about 1.4 at $x = 10d$ to about 1.5 at $x = 20d$. Figure 6 shows C_ε versus Re_λ at $x = 20d$ for both gap ratios.

Notice that while in fig. 5 the data is coloured by x location, in fig. 6 it is coloured by the distance to the centreline (y). Figure 6 highlights the robustness of the power-law, in particular for the $g/d = 2.4$ case where Re_λ first increases and then decreases with increasing distance to the centreline, all the while in close agreement with the fit $C_\varepsilon \propto Re_\lambda^{-p}$.

Interestingly, Chen & Vassilicos (2022) also observed $C_\varepsilon \propto Re_\lambda^{-p}$ with some scatter in the values of p and found $p \approx 1.5$ after removing the dominant POD modes in their data. Our value of $p \approx 1.3$ for $g/d = 1.25$ is also remarkably close to that found in the experiments of Chen & Vassilicos (2022) for the same gap ratio at $x = 7d$ (without the removal of dominant POD modes).

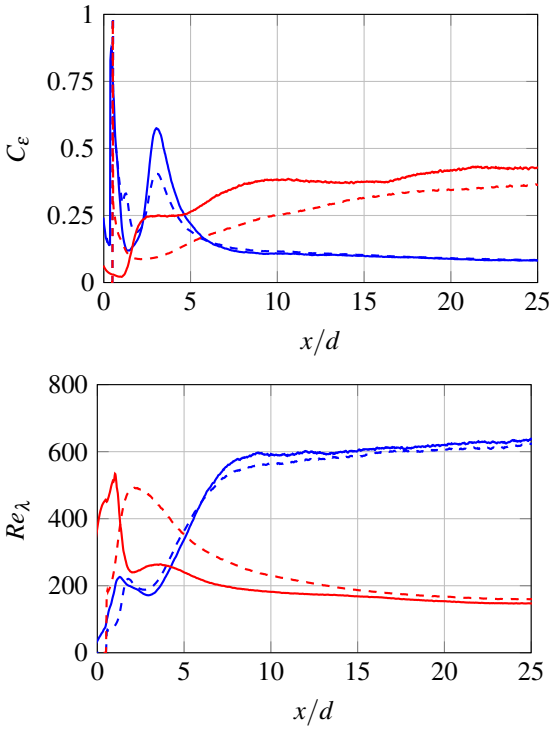

Figure 2: C_ε (top) and Re_λ (bottom) along x at $y = 0$ (full lines) and $y = g/2$ (dashed lines) for $g/d = 1.25$ (blue) and $g/d = 2.4$ (red).

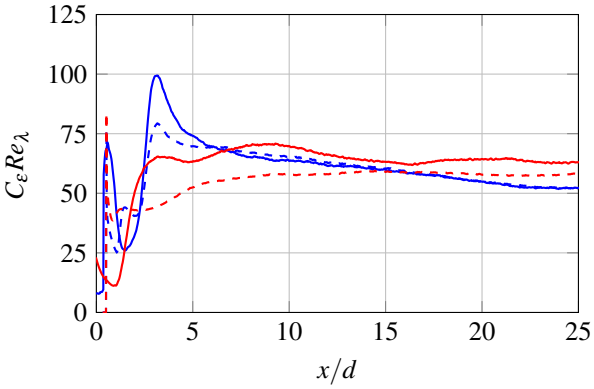

Figure 3: The product $C_\varepsilon Re_\lambda$ along x (see caption of fig. 2 for legend).

Second Order Structure Functions: Scaling and Budget

Having established that C_ε varies in space, following a clear power law dependence on Re_λ, we now turn our attention to the second order structure functions of the streamwise and cross-stream velocity components. These are shown in figs. 7 and 8 and it becomes immediately evident that the $g/d = 1.25$ case does not exhibit clear $2/3$ power laws, whereas the $g/d = 2.4$ case does. In fact, with increasing downstream distance, the plateau in the compensated structure functions becomes evermore evident for $g/d = 2.4$ (even if narrower) whereas for $g/d = 1.25$ there is an increasing departure from any plateau.

Apart from a potential contribution from mean flow (whose significance should reduce with increasing X), it is likely that coherent structures associated with vortex shedding play an important role in figs. 7 and 8. Alves Portela *et al.* (2017) showed how (but see also Thiesset *et al.*, 2014) very intense vortex shedding "contaminates" the scale-space distribution of second order structure functions, potentially obfuscating any underlying power laws (this is particularly true at moderate Reynolds numbers). Indeed, we found (not shown for brevity) that the peak power spectral density (normalised by total energy) of u_2' is *ca.* three orders of magnitude larger for $g/d = 1.25$ than $g/d = 2.4$. Furthermore, the magnitude of this peak decreases with increasing X/d significantly only for $g/d = 2.4$.

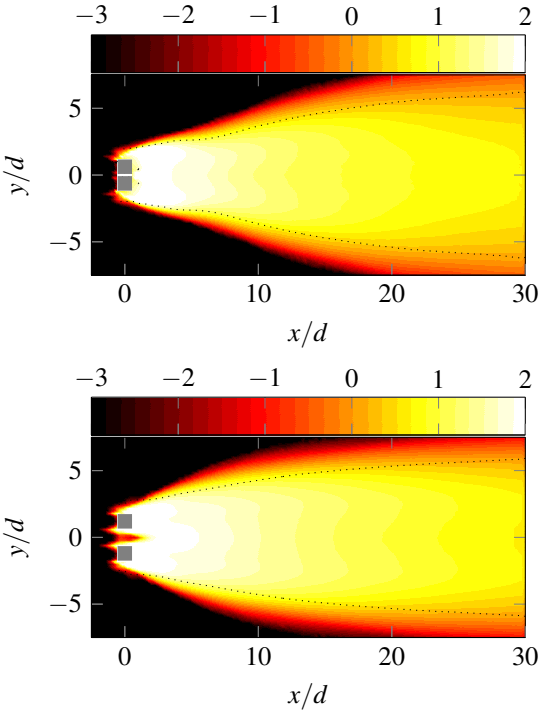

Figure 4: Contour map of $\log(\mathscr{E})$, where $\mathscr{E} = \langle \omega_i \omega_i \rangle$ is the mean enstrophy (and $\boldsymbol{\omega} = \boldsymbol{\nabla} \times \boldsymbol{u}$). The dotted line indicates the y location at which $\mathscr{E}/\max(\mathscr{E}) = 0.25$ at each streamwise position x. Top: $g/d = 1.25$; bottom: $g/d = 2.4$.

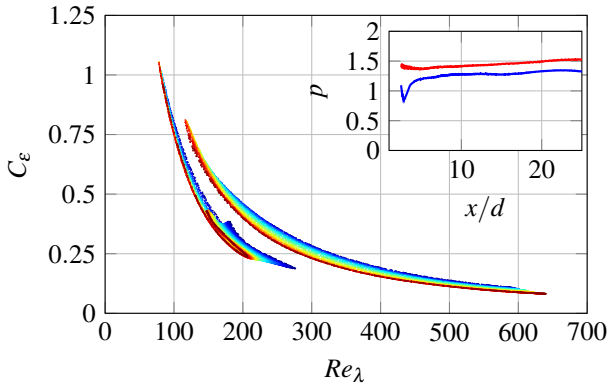

Figure 5: C_ε versus Re_λ for $10 < x/d < 25$ and for y within the dotted lines indicated in fig. 4; the points are coloured by x from blue to red. The leftmost cluster of points corresponds to $g/d = 2.4$ and the rightmost to $g/d = 1.25$. The inset show the exponents p along x for $g/d = 1.25$ (blue) and $g/d = 2.4$ (red).

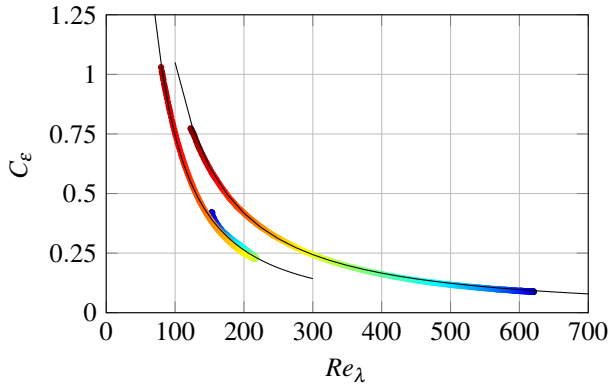

Figure 6: C_ε versus Re_λ at $x = 20d$, the full lines indicate the fits $743Re_\lambda^{-1.5}$ (left) and $480Re_\lambda^{-1.33}$. The leftmost cluster of points corresponds to $g/d = 2.4$ and the rightmost to $g/d = 1.25$.

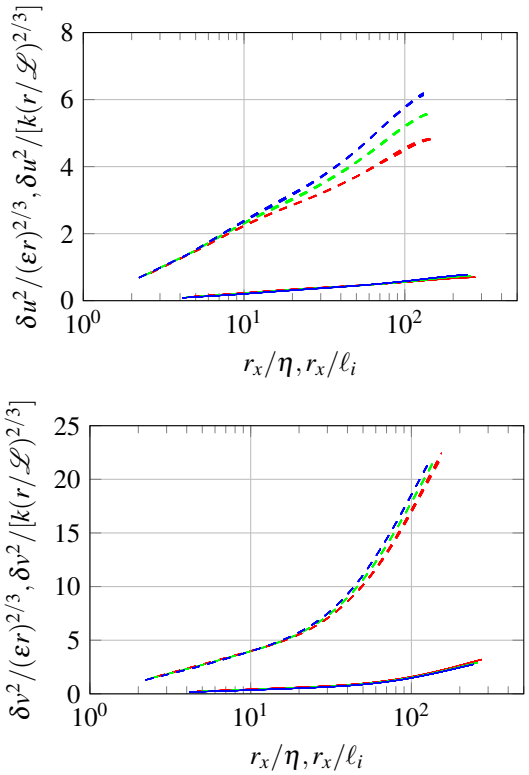

Figure 7: The second order structure functions $\langle(\delta u)^2\rangle$ and $\langle(\delta v)^2\rangle$ normalised both in Kolmogorov variables (dashed lines) and as in eq. (2) (full lines), for $g/d = 1.25$. The colours distinguish between the streamwise locations $X/d = 15$ (red), $X/d = 20$ (green) and $X/d = 25$ (blue); lines of the same colour correspond to different $0 < Y/d < 0.5$.

Focusing on the $g/d = 2.4$ configuration, fig. 8 makes it clear that the normalisation given by eq. (2) collapses more successfully the structure functions at different locations (both X and Y) than Kolmogorov normalisation. We found that further increasing the range of Y over which the curves are plotted deteriorates the collapse. Larger values of Y, however, were found to be associated with stronger mean-flow inhomogeneity, whereas the theory of Chen & Vassilicos (2022) actually

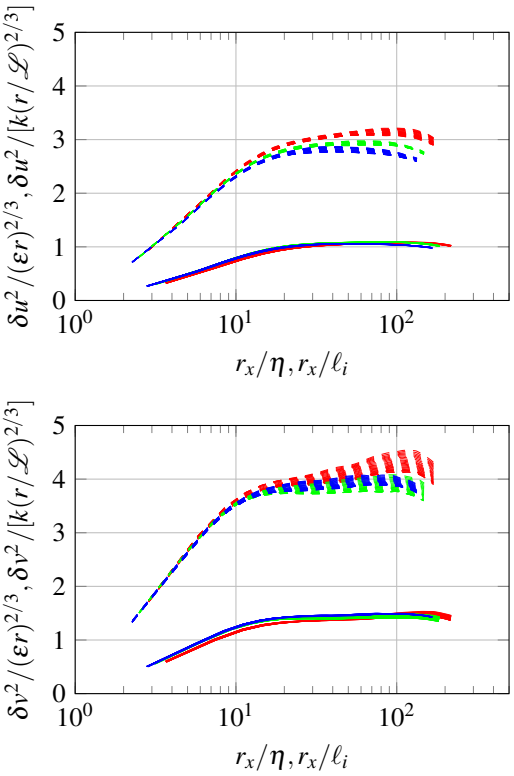

Figure 8: As fig. 7 but for $g/d = 2.4$.

requires that the mean flow is homogeneous: otherwise the non-linear terms in eq. (3) will feature production, which is unlikely to satisfy the same inner/outer scalings as "pure" inter-scale/space transfers.

Figures 9 and 10 shows the terms that feature in eq. (3), except for the viscous diffusion term which is negligible for $r_x \gtrsim \lambda$ (see Valente & Vassilicos, 2015). One can show that inner similarity actually translates to $\propto \sigma\varepsilon_1$, which is why we have plotted (versus r_x/ℓ_i) all terms normalised by $\sigma\varepsilon_1$ in figs. 9 and 10.

Contrasting the budgets of $\langle(\delta u)^2\rangle$ in figs. 9 and 10 reveals that Π_u and $\mathscr{T}_{p,u}$ are qualitatively different between the two configurations. In particular, while for $g/d = 2.4$ $\mathscr{T}_{p,u}$ remains small at all r_x, X and Y investigated here, it is actually one of the dominant terms in the $g/d = 1.25$ case, acting as a source of $\langle(\delta u)^2\rangle$. Conversely, in the $g/d = 1.25$ flow Π_u actually changes sign for some r_x ($\sim 75\ell_i$ at $X = 15, 20d$ and $\sim 200\ell_i$ at $X = 25d$) whereas it remains negative at all r_x for $g/d = 2.4$. In both cases the spatial transport is comparable to the remaining terms in the budget, acting as a source of $\langle(\delta u)^2\rangle$ - actually the only source term for the $g/d = 2.4$.

While the change in sign of Π_u could suggest a reversal in direction of the non-linear cascade in the $g/d = 1.25$ flow, we have checked that $\delta u_1 \delta u_1^2$ is monotonic and negative for all r_x, X and Y considered. This means that in this flow, contributions to Π_u associated with at least one of the terms $\frac{\partial\langle\delta u_2(\delta u_1)^2\rangle}{\partial r_y}$ and $\frac{\partial\langle\delta u_3(\delta u_1)^2\rangle}{\partial r_z}$ introduce sufficient expansion in the cascade (see Vassilicos, 2015; Chen & Vassilicos, 2022, for an interpretation of the non-linear cascade in terms of compression/expansion events), along directions normal to r_x, to overcome the compression occurring along r_x.

Let us now restrict our attention to the $g/d = 2.4$ case, where clear 2/3 power laws were observed in fig. 8. The theory of Chen & Vassilicos (2022) predicts that these power

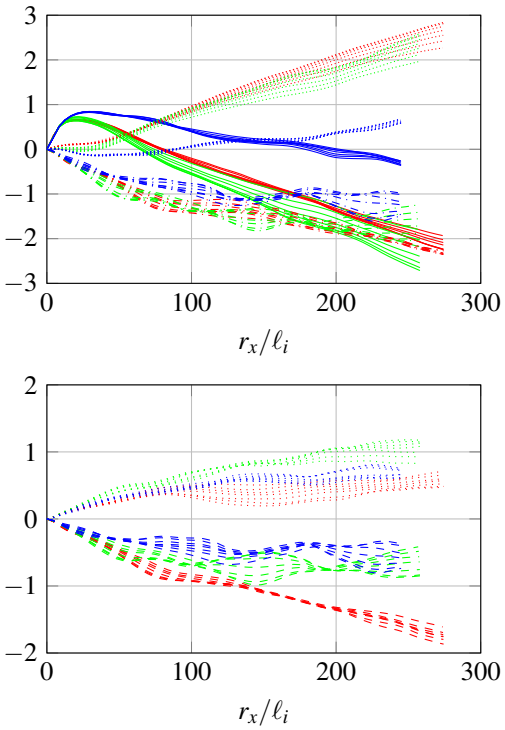

Figure 9: The various terms involved in eq. (3) normalised by $\sigma\varepsilon_1$ for $g/d = 1.25$. Top: minus the interscale transfer $-\Pi_u$ (full line), pressure-velocity correlation $\mathscr{T}_{p,u}$ (dotted line) and total spatial transport $\mathscr{A}_u - \mathscr{T}_u$ (dash-dotted line); bottom: mean flow advection $\mathscr{A}_u$ (dashed line) and turbulent transport $\mathscr{T}_u$ (dotted line). The colours distinguish between the streamwise locations $X/d = 15$ (red), $X/d = 20$ (green) and $X/d = 25$ (blue); lines of the same colour correspond to different $0 < y/d < 0.5$.

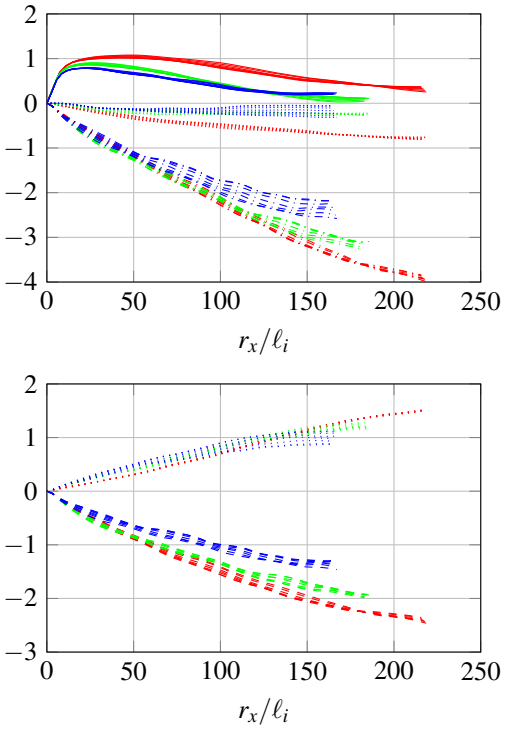

Figure 10: As fig. 9 but for $g/d = 2.4$.

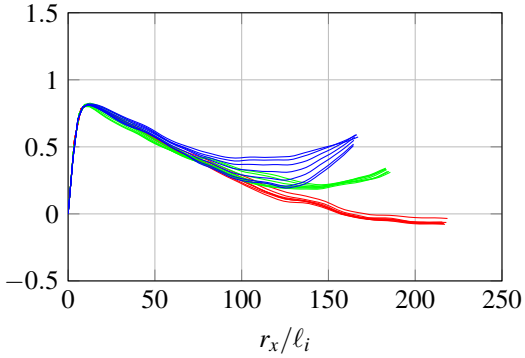

Figure 11: Minus the interscale transfer $-\Pi_v$, normalised by $\sigma\varepsilon_2$. The colours distinguish between the streamwise locations $X/d = 15$ (red), $X/d = 20$ (green) and $X/d = 25$ (blue); lines of the same colour correspond to different $0 < y/d < 0.5$.

laws are associated with self-similarity of the terms involved in eq. (3) in terms of inner and outer scales, whereas the matching between inner and outer budgets further implies that $\Pi_u/\sigma\varepsilon_1 = \text{const.}$ in the intermediate range of scales, assuming of course that such an intermediate range exists and is wide enough.

We do not observe a clear plateau in $\Pi_u/\sigma\varepsilon_1$, except perhaps for $X = 15d$; as X increases (recall from fig. 2 that the local Reynolds number decreases with increasing x), the magnitude of $\Pi_u/\sigma\varepsilon_1$ actually decreases, retaining a peak at $r_x \sim \lambda_z$, a Taylor micro-scale that uses only span-wise information (which we found to better represent the scale above which $\mathscr{D}_u$ is negligible). Notice that the theory implies that $\mathscr{A}_u$ becomes negligible in the inner balance of $\langle(\delta u)^2\rangle$ with increasing Reynolds number. It is certainly not the case that $\mathscr{A}_u$ is negligible here, which may be a Reynolds number effect. However, we also find that the spatial regions with largest Re_λ (e.g. $x/d < 15$ but also $y/d > 0.5d$) correspond to regions where mean flow inhomogeneity becomes significant, which is not accounted for in the theory. As already mentioned, the theory deals with inhomogeneity of the turbulence but not of the mean flow.

It is worth noting that $\Pi_v/\sigma\varepsilon_2$ (shown in fig. 11 and corresponding to $v \equiv u_3$) does also not display a clear plateau, despite $\langle(\delta v)^2\rangle$ displaying clear 2/3 power laws. However, in contrast to Π_u, we find that for $r_x/\ell_i \lesssim 100$ the $\Pi_v/\sigma\varepsilon_2$ are all independent of x which indicates that Π_v is self-similar at the inner scales.

CONCLUSION

In this work we have performed DNS of two turbulent wakes generated by pairs of prisms in configurations similar to the experiments of Chen *et al.* (2021). Our results allowed us to confirm some of the assumptions made in their data analysis (owing to experimental limitations), such as small scale axisymmetry.

We have put the observations of Chen *et al.* (2021) to the test by exploring the flow along much broader regions in space. Namely, we have found that power laws of the type $C_\varepsilon \propto Re_\lambda^{-p}$ exist over practically the whole breadth of the mean wake and that the exponent p is actually quite robust, showing only little dependence on stream-wise location. The two configurations analysed yield different exponent p, but they also differ drastically in terms of the streamwise evolution of C_ε and

Re_λ: whereas a familiar non-equilibrium relation develops for $x/d \gtrsim 10$ in the $g/d = 2.4$ case (where Re_λ decreases with increasing x), the smaller gap ratio ($g/d = 1.25$) actually leads to C_ε decreasing at a much faster rate with x than the increase in Re_λ.

We observed $2/3$ power laws in $\langle(\delta u_1)^2\rangle$ and $\langle(\delta u_2)^2\rangle$, the second order structure functions associated with the streamwise and cross-stream velocity components, respectively, for separations aligned with x only for the larger gap ratio $g/d = 2.4$; we expect that the much stronger coherent structures observed in the $g/d = 1.25$ case may be the source of this difference. The terms involved in the energy budget of these quantities are also qualitatively very different between the two flows.

Concerning the different energy budgets of $\langle(\delta u_1)^2\rangle$ between the two flows, in the smaller gap ratio case there is an inversion in the sign of the non-linear inter-scale transfer attributable to expansion events in the directions normal to r_x. Further investigation of this phenomenon will require analysing the cascade along the r_y and r_z directions.

In an assessment of the inhomogeneous turbulence theory of Chen & Vassilicos (2022) in the $g/d = 2.4$ case, we find that mean flow advection is not negligible at small scales owing to the moderate Reynolds numbers. In order to investigate regions of these flows with much larger local Reynolds number it becomes necessary to either simulate higher global Reynolds numbers, which is computationally very challenging, or extend the theory to account for inhomogeneity in the mean flow given that the local Reynolds number is highest in these regions.

ACKNOWLEDGEMENTS

This work is supported by JCV's Chair of Excellence Co-PreFlo funded by I-SITE-ULNE (grant number R-TALENT-19-001-VASSILICOS); MEL (grant number CONVENTION-219-ESR-06) and Region Hauts de France (grant number 20003862).

REFERENCES

Alves Portela, F., Papadakis, G. & Vassilicos, J. C. 2017 The turbulence cascade in the near wake of a square prism. *Journal of Fluid Mechanics* **825**, 315–352.

Bartholomew, P., Deskos, G., Frantz, R. A. S., Schuch, F. N., Lamballais, E. & Laizet, S. 2020 Xcompact3d: An open-source framework for solving turbulence problems on a cartesian mesh. *SoftwareX* **12**, 100550.

Chen, J. G., Cuvier, C., Foucaut, J-M., Ostovan, Y. & Vassilicos, J. C. 2021 A turbulence dissipation inhomogeneity scaling in the wake of two side-by-side square prisms. *Journal of Fluid Mechanics* **924**.

Chen, J. G. & Vassilicos, J. C. 2022 Scalings of scale-by-scale turbulence energy in non-homogeneous turbulence (under review). *Journal of Fluid Mechanics* .

Gautier, R., Laizet, S. & Lamballais, E. 2014 A dns study of jet control with microjets using an immersed boundary method. *International Journal of Computational Fluid Dynamics* **28** (6-10), 393–410.

George, W. K. & Hussein, H. J. 1991 Locally axisymmetric turbulence. *Journal of Fluid Mechanics* **233**, 1–23.

Kraichnan, R. H. 1974 On kolmogorov's inertial-range theories. *Journal of Fluid Mechanics* **62** (2), 305–330.

Lamballais, E., Fortuné, V. & Laizet, S. 2011 Straightforward high-order numerical dissipation via the viscous term for direct and large eddy simulation. *Journal of Computational Physics* **230** (9), 3270–3275.

Ortiz-Tarin, J. L., Nidhan, S. & Sarkar, S. 2021 High-reynolds-number wake of a slender body. *Journal of Fluid Mechanics* **918**.

Thiesset, F. & Danaila, L. 2020 The illusion of a Kolmogorov cascade. *Journal of Fluid Mechanics* **902**.

Thiesset, F., Danaila, L. & Antonia, R. A. 2014 Dynamical interactions between the coherent motion and small scales in a cylinder wake. *Journal of fluid mechanics* **749**, 201–226.

Valente, P. C. & Vassilicos, J. C. 2015 The energy cascade in grid-generated non-equilibrium decaying turbulence. *Physics of Fluids* **27** (4), 045103.

Vassilicos, J. C. 2015 Dissipation in turbulent flows. *Annual Review of Fluid Mechanics* **47**, 95–114.

Zhou, Y., Nagata, K., Sakai, Y. & Watanabe, T. 2019 Extreme events and non-kolmogorov $-5/3$ spectra in turbulent flows behind two side-by-side square cylinders. *Journal of Fluid Mechanics* **874**, 677–698.